www.czasopisma.pan.pl PAN www.journals.pan.pl
Chemical and Process Engineering 2021, 42 (2), 173–190
DOI: 10.24425/cpe.2021.138923

Experimental and numerical investigation of axial and tangential forces in a stirred tank with yield-stress fluids

Anna Story*, Grzegorz Story, Zdzisław Jaworski

West Pomeranian University of Technology in Szczecin, Faculty of Chemical Technology and Engineering, Department of Chemical and Process Engineering, al. Piastów 42, 71-065 Szczecin, Poland

Complex rheological properties of yield-stress materials may lead to the generation of an intensive mixing zone near a rotating impeller. From the practical point of view, the zone should cover most of the stirred liquid. According to the literature review, several parameters may affect the size of the mixing zone, in particular forces exerted on the liquid. This paper presents both experimental and numerical investigation of axial and tangential forces generated during mechanical mixing of yield-stress fluids in a stirred tank. The tested fluids were aqueous solutions of Carbopol Ultrez 30 of concentration either 0.2 or 0.6 wt% and pH = 5.0. The study was performed for three types of impeller, pitched blade turbine, Prochem Maxflo T and Rushton turbine, in a broad range of their rotational speed, $N = 60 - 900$ rpm. The axial and tangential forces were calculated from the apparent mass of the stirred tank and torque, respectively. The experimental results were compared with CFD predictions, revealing their good agreement. Analysis of the generated forces showed that they are dependent on the rheological characteristic of liquid and the impeller type. It was also found that although axial force was smaller than tangential force, it significantly increased the resultant force.

Keywords: mixing, yield-stress fluid, axial force, tangential force, CFD

1. INTRODUCTION

Materials which behave either as fluids or solids, depending on the applied shear stress, are called yield-stress or viscoplastic fluids and they are typical representatives of soft matter. Different mixtures are ranked by physicists among the yield-stress fluids (YSF), e.g., microgels, colloidal suspensions, emulsions, foams and granular suspensions (Bonn et al., 2017). Microgels are defined as aqueous dispersions of cross-linked acid-containing lattices (Rodriguez et al., 1994). Carbopol (carbomer) microgels have been widely used in research as model yield-stress fluids. Their rheological characteristics should be measured in specific conditions and the steady-state dependence of shear stress vs. shear rate is well described by the Herschel–Bulkley (H–B) model (Jaworski et al., 2021). The model name is given after the authors (Herschel and Bulkley, 1926). In the model, shear stress, τ, exerted on a material depends on the material yield stress, τ_y, and the rate of shear, $\dot{\gamma}$, using two empirical constants, k and n.

$$\tau = \tau_y + k\dot{\gamma}^n \tag{1}$$

* Corresponding author, e-mail: Anna.Story@zut.edu.pl

Stirring of yield-stress materials is often associated with formation of an intensive circulation zone around a rotating stirrer, while the rest of the material remains stationary. The well-mixed zone was originally named cavern (Wichterle and Wein, 1975). Nevertheless, typical devices used to process yield-stress materials are stirred tanks and the avoidance of cavern formation is crucial in successful mixing (Simmons et al., 2009). The size and shape of a cavern depends on the stirrer-tank geometry, the impeller rotational speed and the rheological flow curve of the material (Story and Jaworski, 2017).

In the design of stirred tanks for yield-stress materials, a range of quantitative data is required. Among them are the predicted diameter and height of caverns created in a given tank and stirred liquid. A typical way to estimate the cavern dimensions is from models based on experimental results. A comprehensive presentation of such models to evaluate the cavern size and shape was presented by Xiao et al. (2014). All the models employed the following independent variables: the Herschel–Bulkley (H–B) parameters, stirrer type, its diameter and rotational speed. Those variables determine the tangential and axial forces exerted by the stirrer, with the former derived from stirrer power characteristics, and the latter from axial force correlations in the case of axially pumping impellers (Story et al., 2018). More advanced empirical models of caverns use a resultant force of the tangential and axial forces (Xiao et al., 2014).

Two determination methods, i.e. experimental and numerical, of the axial and tangential forces have been published in the subject literature. An extensive body of information has been made available on the torque necessary to rotate impellers with the first quantitative reports in 1950s (Stręk, 1981). The impeller torque can be measured with a range of techniques, either directly at the impeller shaft or indirectly as the tangential reaction force at the tank wall and bottom. The impeller torque has been most often correlated in the form of the power number, *Po* vs. Reynolds number, Re (Stręk, 1981). The measurement methodology of the impeller torque in the YSF has been the same as in other fluids. Similarly to the tangential force, the axial component can also be measured as the primary force exerted by a stirrer on the liquid or as the secondary one exerted by the liquid on the vessel wall and bottom (Fořt et al., 2013; Wu and Pullum, 2000). More information on the experimental methods of measuring tangential and axial forces for non-Newtonian fluids can be found elsewhere (Story et al., 2018).

The measurement methods of the two forces have also been applied to stirring of yield-stress fluids. The tangential force, usually expressed in the form of power draw in YSF, was measured in a range of stirrer-tank configurations (Amanullah et al., 1997; Amanullah et al., 1998; Bhole and Bennington, 2010; Bhole et al., 2011; Galindo et al., 1996; Galindo and Nienow, 1992; Nienow and Elson, 1988; Story and Jaworski, 2017). The stirrer axial force has been less frequently investigated since the force is associated with inclined stirrer blades and the first advanced report about yield-stress fluids appeared in 1998 (Amanullah et al., 1998). Later on, axial thrust in pulp suspensions with yield-stress was studied by Bhole and Bennington (2010), Bhole et al. (2011), Hui et al. (2009), who used side-entering axial-flow impellers. The axial force measurements were used in determination of cavern models and also in validation of CFD predictions. A similar approach to build a model and validate CFD simulations was also applied in standard stirred tanks with a PMT hydrofoil impeller (Story and Jaworski, 2017; Story et al., 2018).

The key feature of mathematical modelling with Computational Fluid Dynamics (CFD) is a numerical solution to the set of 3D partial differential equations of the mass and momentum balance for a flowing fluid. That modelling technique has been successfully developing since 1980s. Exemplary details of the numerical procedure are presented in Section 3. In parallel to determination of the velocity field, the two forces exerted by stirrers on yield-stress materials can also be derived from numerical predictions. The last two decades were rich in papers reporting on CFD predictions of viscoplastic flow and of cavern formation in stirred tanks, which was initiated by Adams and Barigou (2007). Most authors of CFD modelling of yield-stress flows assume the flows of viscoplastic materials are laminar, with two exceptions (del Pozo et al., 2020; Xiao et al., 2014). Following the typical approach, laminar flow of the stirred liquid is assumed in this study. Theoretically, apparent viscosity of the material in stagnant zone, where the shear stress $\tau < \tau_y$,

should be infinite and such a value would result in a lack of convergence of numerical solutions. A frequent solution to avoid numerical divergence is a selected viscosity regularization (Frigaard and Nouar, 2005). One of the approaches, that is used in this present study, is to calculate apparent viscosity, $\mu_{\text{app}} = \tau/\dot{\gamma}$, directly from Eq. (1) for shear rates higher than a threshold rate, $\dot{\gamma}_t$, for which the apparent viscosity is equal to $\mu_t = \tau_t/\dot{\gamma}_t$. For lower shear rates, the apparent viscosity is estimated from a linear relationship, Eq. (2), where A and B are positive constants dependent on the shear rate.

$$\mu_{\text{app}} = A\mu_t + B \tag{2}$$

A variety of CFD studies were published on stirring of yield-stress fluids, both without parallel experiments (Ameur, 2016; 2017; 2019; Ameur et al., 2011; Bakker et al., 2009; 2010; Dylak and Jaworski, 2015; Ford et al., 2006; Savreux et al., 2007; Sossa-Echeverria and Taghipour, 2014; 2015) and also as joint experimental-CFD studies (Adams and Barigou, 2007; Arratia et al., 2006; Kelly and Gigas, 2003; Russell et al., 2019; Story and Jaworski, 2017; Xiao et al., 2014). However, a dual experiment-CFD work dedicated to the axial and tangential forces in Carbopol microgel stirred by the radial or axial or mixed type impeller has not been found in the literature. Finally, it should be emphasised that the magnitude of axial and tangential forces exerted by impellers are key factors in designing stirred tanks.

2. EXPERIMENTAL STUDY

2.1. Experimental rig

Experimental studies were performed in a flat-bottomed cylindrical stirred tank (Fig. 1) of a diameter $T = 0.190$ m, equipped with one of three high-speed impellers: down pumping pitched blade turbine (PBT), Prochem Maxflo T (PMT) or Rushton turbine (RT), each of a diameter $D = 0.078$ m. Pictures of the impellers together with schemes containing their basic dimensions are presented in Figure 2.

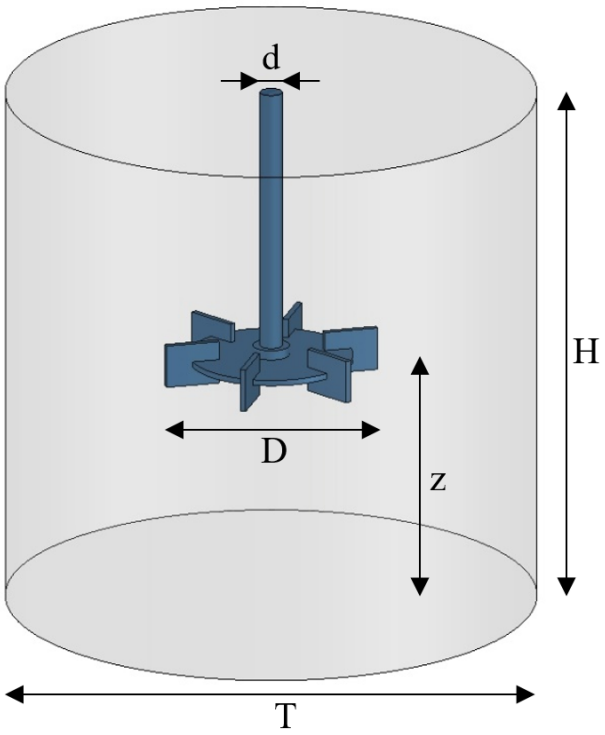

Fig. 1. Geometrical parameters of stirred tank

The impellers were selected in such a way that each of them generated a different primary circulation of the liquid in the tank, i.e. PMT impeller provided mainly axial, RT impeller mainly radial, and PBT impeller mixed axial-radial circulation of the liquid inside the tank. The impellers were placed coaxially with the tank and at a distance of $z = 0.45T$ from its bottom. The shaft diameter was equal to $d = 0.008$ m. The mixing tank was filled to a height $H = D$ with aqueous solutions of Carbopol Ultrez 30 grade, a commercial polyacrylic acid produced by Lubrizol Company (Wickliffe, Ohio, USA). Two concentrations of CU30 were tested, either 0.2 and 0.6 wt% in distilled water. Measurements were carried out for a wide range of rotational impeller speed, $N = 60 - 900$ rpm.

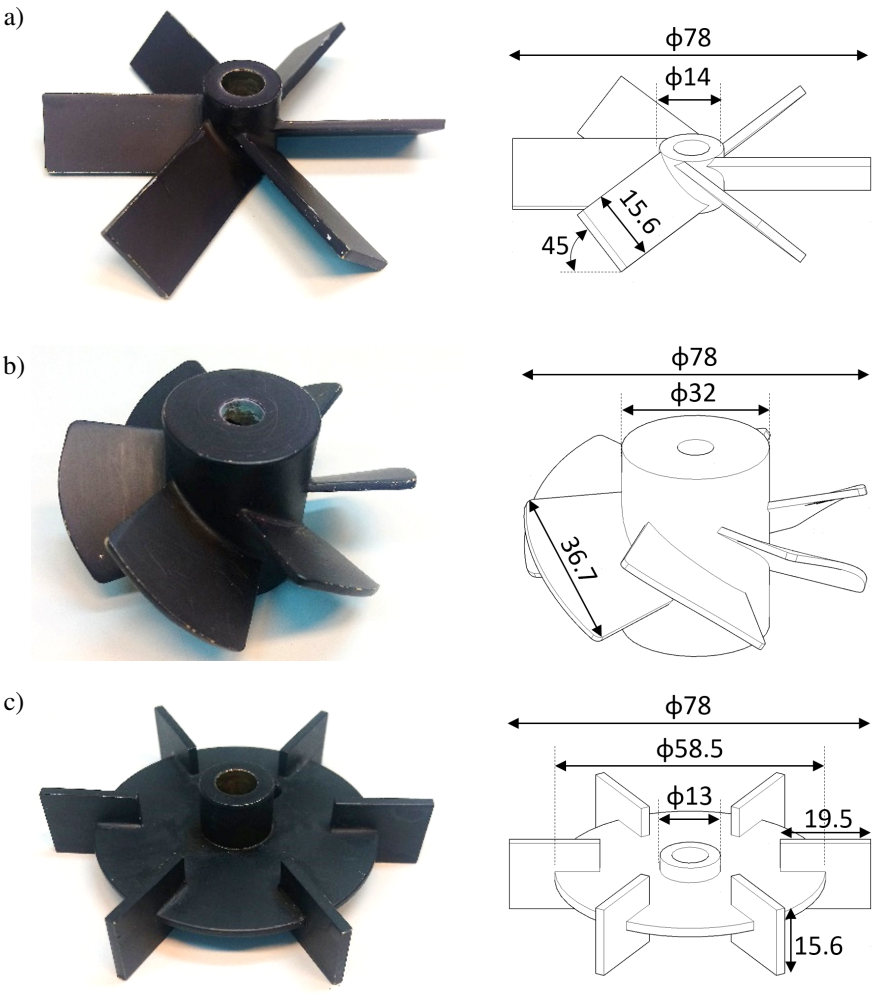

Fig. 2. Tested impellers: a) pitched blade turbine, b) Prochem Maxflo T, c) Rushton turbine

2.2. Preparation of tested fluids

Preparation of the tested fluids, two Carbopol Ultrez 30 microgels with concentrations, c_{CU30}, of 0.2 and 0.6 wt%, was carried out in two stages. The first stage consisted in the preparation of aqueous CU30 suspensions with strictly defined concentrations. In order to ensure even dispersion of the polymer powder in the distilled water, both components were mixed for a minimum of 3 hours using an electronic overhead stirrer (IKA, Eurostar power control-visc; IKA-Werke GmbH&Co. KG, Staufen, Germany) and a paddle impeller that rotated with a speed of 300 rpm.

In the second stage CU30 suspensions were gradually neutralized with 1 M sodium hydroxide (NaOH) to pH = 5.0 which resulted in transparent and high-viscosity microgels with different values of apparent viscosity. During the neutralization, the prepared liquids were mixed for a minimum of 5 hours with impeller

speed increasing to 900 rpm. Changes in pH were continuously controlled using pH & Ion-Meter GLP 22+ (Crison) and a 5021T sensor probe that was constantly immersed in the prepared liquid. The pH value was considered stable when it did not change by 0.01 within 10 minutes. More detailed information about fluid preparation can be found in (Story et al., 2020).

2.3. Rheological characteristic

Rheological measurements of prepared liquids were taken about 24 hours after their preparation. Flow characteristics, i.e. shear stress, τ, vs. shear rate, $\dot{\gamma}$, were measured using the MCR 102 rheometer (Anton Paar) equipped with a sandblasted cone-plate (CP50-1/S) measuring system with the roughness of 4 to 7 μm, to avoid wall slip. During the rheological tests, the temperature of the microgel samples was kept constant at t = 20.5 °C by means of a Peltier temperature module and the measuring system was surrounded by a humidifying chamber filled with warm water to prevent evaporation of the sample. Each of the measurements of rheological properties was preceded by one-minute pre-shear and five minutes of relaxation of the loading stress. Regular measurements were carried out for a logarithmically increasing wide range of shear rate, $\dot{\gamma} = 10^{-5}$–10^{3} s^{-1}, applying six measurement points per every decade. The apparent viscosity, μ_{app}, of the studied liquids and also their flow curves are presented in Fig. 3.

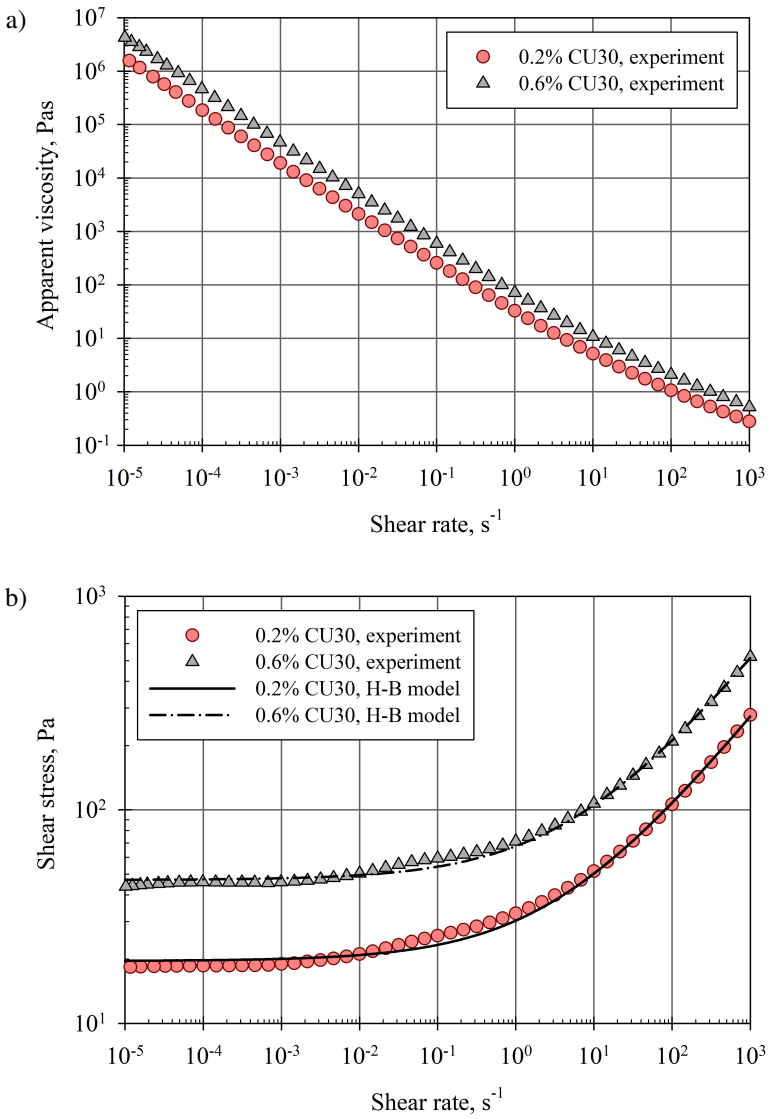

Fig. 3. Apparent viscosity (a) and flow curves (b) of tested CU30 microgels differing in concentration

As can be seen from the charts, the apparent viscosity (Fig. 3a) of the microgels decreased with increasing value of $\dot{\gamma}$ and ranged from $2.8 \cdot 10^{-1}$ to $7.6 \cdot 10^{6}$ Pa·s. Moreover, higher values of μ_{app} were observed for the higher polymer concentration for the whole tested range of $\dot{\gamma}$. The flow curves (Fig. 3b) indicate that both microgels exhibit complex, non-linear rheology combined with a yield point. Such flow characteristic can be described using Herschel–Bulkley model. Therefore, based on the experimental results, values of three rheological parameters of the H–B model: yield stress, τ_y, consistency coefficient, k, and flow index, n, were estimated. They are collected in Table 1. The theoretical flow curves resulting from H–B model were plotted in Figure 3b. In order to assess the quality of the theoretical model, values of the determination coefficient were determined, obtaining $R^2 = 0.9991$ for both microgels. Therefore, it can be concluded that the applied H–B model adequately reproduces the experimental data. Due to numerical simulations carried out in this study, it was necessary to determine the critical shear rate, $\dot{\gamma}_y$, i.e. the intersection of the $\tau = \tau_y$ and $\tau = k\dot{\gamma}^n$ lines, denoting the conventional point of balancing of elastic (solid) and viscous (liquid) forces. Values of $\dot{\gamma}_y$ are also presented in Table 1.

Table 1. Herschel–Bulkley model parameters for tested CU30 microgels

c_{CU30}, %	τ_y, Pa	k, Pa·s^n	n	R^2	$\dot{\gamma}_y$, s^{-1}
0.2	19.6	10.7	0.459	0.9991	3.7386
0.6	47.0	20.7	0.451	0.9991	6.1608

2.4. Tangential force

The tangential forces, f_φ, generated by the tested impellers were determined as in the previous paper by the authors (Story et al., 2018) from the primary torque, T_o, exerted on the stirred liquid by the impeller blades, disc, hub and shaft. Measurements of the primary torque were performed using the IKA®EUROSTAR PowerControl-Visc device, equipped with the torque measurement module. The measuring device was connected to a computer with Labworldsoft software that allowed to set the rotational impeller speed as well as to monitor and record the measuring data. During measurements, the temperature of microgels was kept at a constant level of $t = 20.5 \pm 0.5$ °C. For each impeller type and every tested impeller speed from the range of $N = 60 - 900$ rpm, a minimum of 100 instantaneous values of the primary torque, $T_{o,i}$, were recorded and then averaged. According to the simplified literature approach (Amanullah et al., 1998), the total values of the impeller tangential force were calculated, as $f_\varphi = 4T_o/3R$, where R is the impeller radius. Tangential forces are presented in Figure 4a as a function of mixing power, $P = 2\pi NT_o$. The average values of primary torque were also used to calculate the dimensionless power number, $Po = 2\pi NT_o/(N^3D^5\rho)$, plotted in Figure 4b, as a function of the generalized Reynolds number, $\mathrm{Re} = ND^2\rho/\mu_{app}$. Values of the Reynolds number for tested non-Newtonian yield stress fluids were calculated applying the apparent viscosity estimated from the H–B model and Metzner–Otto coefficient (Jaworski and Nienow, 1994; Story et al., 2018).

Analysing the tangential forces presented in Figure 4a it was concluded that for all tested mixing tanks and both microgel concentrations their values increased with increasing value of power draw. However, the increase was less than directly proportional since $f_\varphi \sim P/N$. Taking into account three tested types of impellers, the turbine with pitched blades was always the one that generated the smallest tangential forces. On the other hand, the highest values of f_φ were observed usually for the PMT type impeller. However, for 0.2% CU30 microgel and mixing power higher than $P = 5$ W, the Rushton turbine produced the maximum f_φ. Evaluating the effect of the microgel concentration on the generated tangential forces it should be noted that initially they reached higher values for 0.6% polymer concentration. However, there was a certain value of power draw of $P = 10$ W for which the difference between f_φ produced in both liquids had faded.

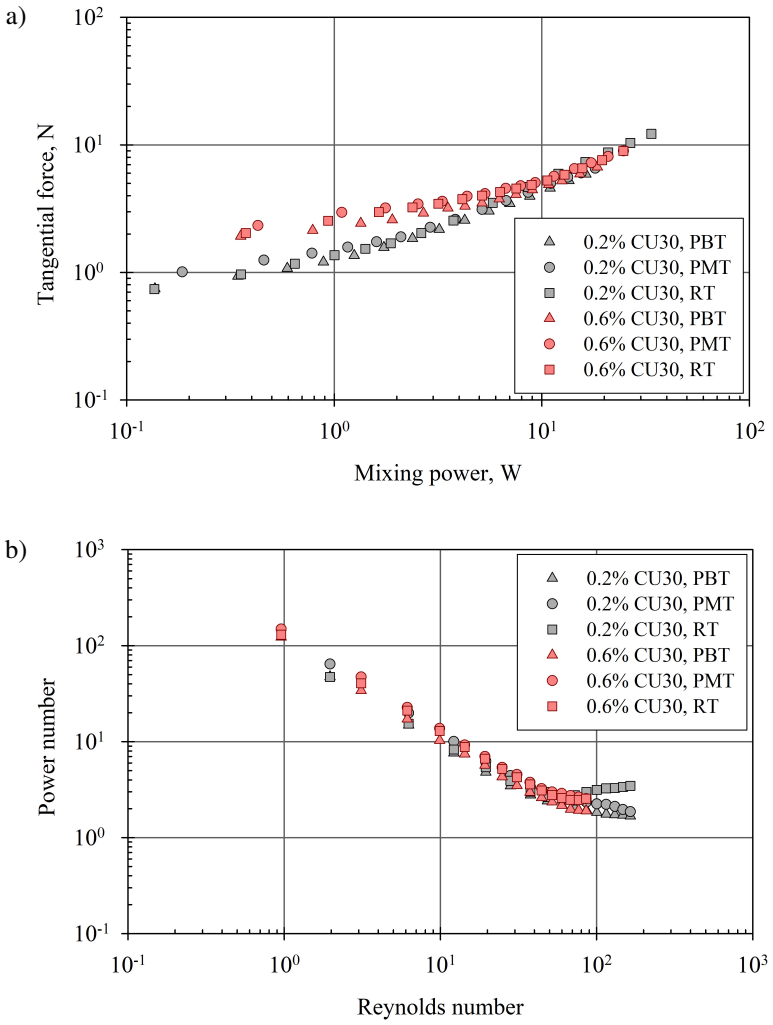

Fig. 4. Tangential forces generated by the impellers (a) and mixing power characteristics (b) of studied systems. Experimental data

It follows from the presented power curves (Fig. 4b) that measurements were carried out for laminar and early transitional fluid flow. In the laminar flow range, i.e. for Reynolds number up to about 40, the power number decreased with increasing Reynolds number. Also, all power curves for this Re range can be approximated with one straight line with a slope of $a = -0.995$. In the transitional flow range, however, there is a significant difference between the power characteristic of the three types of impellers. Compared to the laminar flow regime, the power number still decreases for the PBT and PMT impellers, while for the radial RT impeller it increases. Such a dependence is similar to that of Newtonian fluids.

2.5. Axial force

The axial forces, f_{ax}, in the mixing tank were determined by measurements of apparent mass, Δm, i.e. the difference between the mass of the filled mixing tank with a rotating and stationary impeller. The mass difference multiplied by the gravitational acceleration corresponds to the change in generated axial force (Story et al., 2018). Measurements were carried out using an electronic weighing scale WPT 24C RADWAG® of the maximum load of 24 kg and the measuring accuracy of 1 g. The conditions and process parameters (i.e. temperature, rotational impeller speed) set during the measurements of the apparent mass of the mixing tank were the same as in torque measurements. Like previously, the scale was connected to a computer that enabled monitoring and recording a minimum of 100 instantaneous values of apparent mass,

which were averaged and taken for further analysis. It should be emphasized that for the tested high-viscosity CU30 microgels, the axial force expressed by Δm was practically constant during the measurement or it changed to a maximum of ±1 g, depending on the impeller speed. The total axial force for a given impeller speed was calculated as the product of apparent mass difference and the acceleration due to gravity. Axial forces are presented in Fig. 5a as a function of mixing power, P. Based on the total axial force, the dimensionless thrust number was calculated for the PBT and PMT impellers, as $Th = f_{ax}/(N^2D^4\rho)$, and plotted in Fig. 5b as a function of Reynolds number. It should be emphasized that the measurements and analysis of axial forces were performed only for two of the three tested impellers, i.e. PBT and PMT, since the Rushton turbine, as an agitator generating a typically radial circulation of liquid in the tank, did not exert measurable axial thrust.

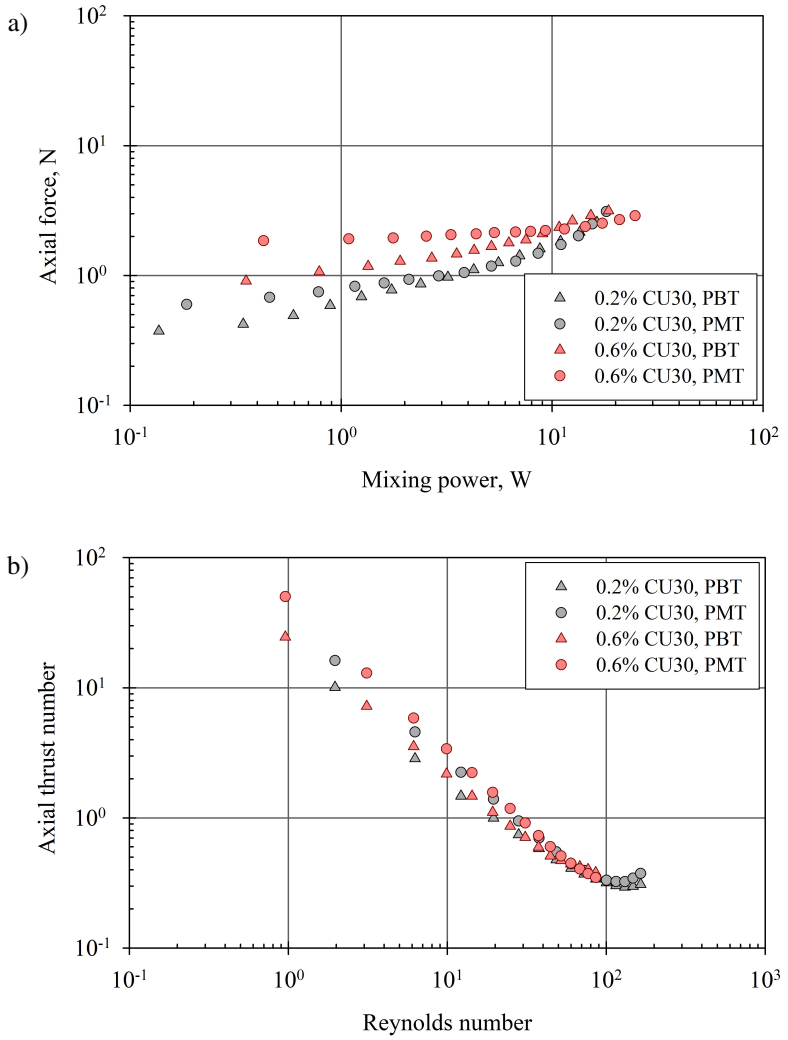

Fig. 5. Axial forces generated by the impellers (a) and dimensionless axial thrust number (b). Experimental data

Analysing the data presented in Fig. 5a, it was found that the axial forces increased with growing power draw. However, as in the case of tangential forces, the increase was less than directly proportional. A considerable influence was observed of both the type of impeller and the concentration of the microgel on the value of the generated axial force. Generally, higher values of f_{ax} were observed for the PMT impeller and 0.6% CU30. The differences between plotted axial forces were relatively large for low values of mixing power and decreased with increasing P. It was found that for 0.2% CU30 and $P > 3.8$ W, the axial forces generated by the PMT and PBT impellers were practically the same, while for 0.6% CU30 and $P > 10$ W axial forces generated by the PBT impeller were higher than those generated by the PMT.

From the graph showing the axial thrust number as a function of the Reynolds number (Fig. 5b) it follows that there is a small influence of the rheological properties on the axial thrust number (for a given impeller), with a significant influence of the impeller type. Among the two tested agitators, higher values of *Th* were observed for PMT. However, for all tested configurations of mixing tanks and microgels, the qualitative trend of axial thrust characteristics was very similar – first decreasing, and increasing from about Re = 140. Contrary to the case of power number, higher differences between *Th* values for tested mixing tanks were observed in the laminar flow range, while they were negligibly small for the transitional regime, i.e. for Re > 40.

2.6. Resultant force

For two impellers that generate the axial force during stirring, the resultant forces, F, were calculated as a root of the sum of the squares of the tangential and axial forces, for the whole tested range of impeller speeds. Obtained results were presented graphically in Figs. 6a–6d, separately for each impeller and polymer concentration.

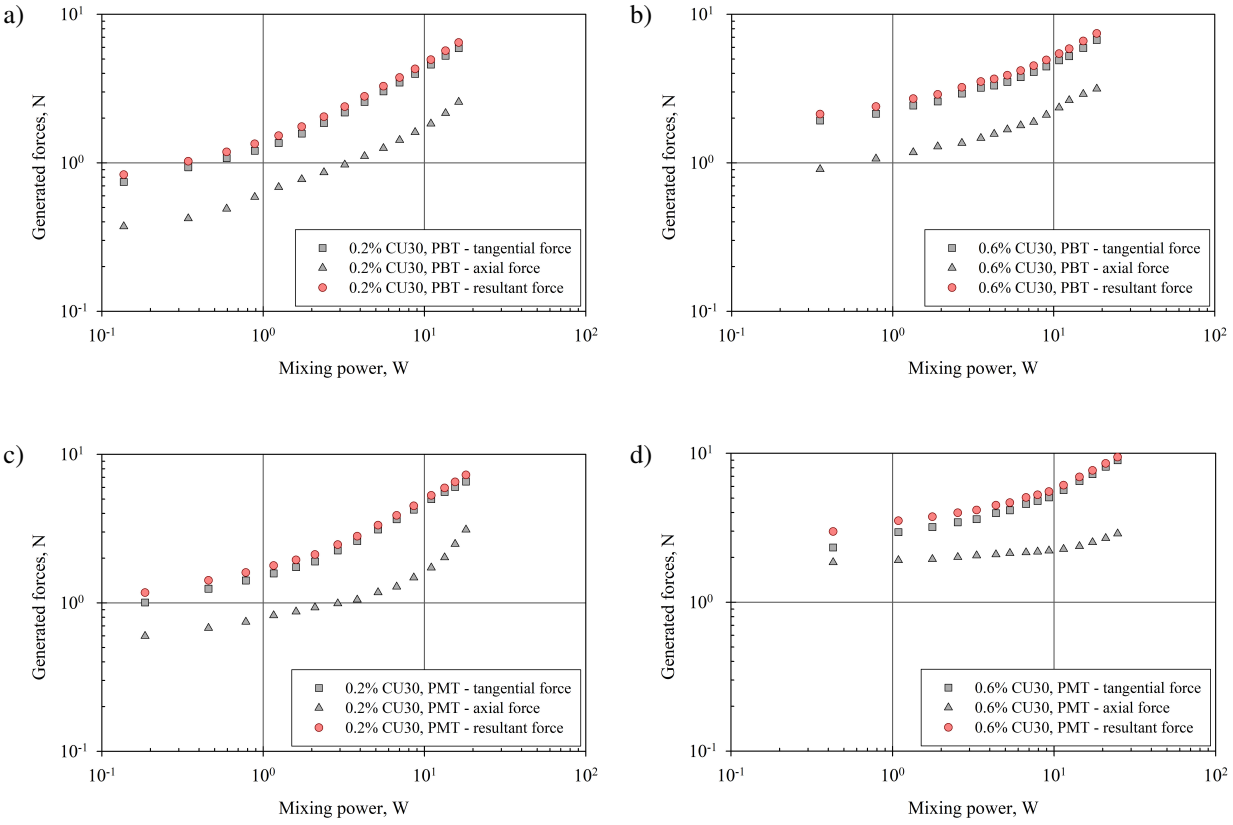

Fig. 6. Values of resultant, tangential and axial forces generated in tested mixing tanks: a) 0.2% CU30, PBT impeller, b) 0.6% CU30, PBT, c) 0.2% CU30, PMT, b) 0.6% CU30, PMT

It follows from the data presented in Fig. 6 that although the axial force takes values smaller than the tangential force, it affects the increase of the resultant force value and, consequently, fluid circulation in the tank. Quantitative analysis showed that the resultant force for 0.2% CU30 was approximately 9.6% and 9.7% higher than the tangential force for the PBT and PMT type impeller, respectively. For 0.6% polymer concentration the calculated growth of F was even higher, i.e. 10.9% and 12.0% for the PBT and PMT type impellers.

3. NUMERICAL SIMULATIONS

3.1. Methodology

Numerical simulations were carried out for the same mixing tanks for which experimental studies were performed. At the pre-processing stage, three geometries of the flow domain were created (one for each impeller type) using ANSYS DesignModeler v. 19.0 software for which numerical grids were generated using ANSYS Meshing v. 19.0 software. The basic characteristics of the generated meshes together with parameters that define their quality are summarized in Table 2. Due to the complex geometry of the flow domains, especially in the region near the impeller, all generated meshes were unstructured and build from tetrahedral computational cells. Analysis of the grid parameters such as skewness, aspect ratio and element quality showed that the generated meshes have good quality and can be used in numerical simulations.

Table 2. Characteristics of generated numerical meshes

Numerical grid	*1*	*2*	*3*
Type of impeller	PBT	PMT	RT
Type of computational cells	tetrahedral	tetrahedral	tetrahedral
Number of computational cells	652 582	713 597	764 705
Skewness, average and (maximum) values	0.21 (0.83)	0.22 (0.82)	0.21 (0.84)
Aspect ratio, average and (maximum) values	1.80 (10.1)	1.82 (10.2)	1.80 (10.5)
Element quality, average and (minimum) values	0.85 (0.22)	0.84 (0.22)	0.85 (0.21)

Numerical simulations of non-Newtonian yield-stress fluids flow were performed by means of the Computational Fluid Dynamic (CFD) technique using the commercial ANSYS Fluent v. 19.0 software. This software allowed to numerically solve the set of differential balance equations for the steady-state momentum transport and continuity with assumptions of the constant density of the stirred CU30 microgels and their apparent viscosity determined on the basis of the Herschel–Bulkley model, with the rheological parameters estimated from experimental data (Table 1). In order to avoid the discontinuity in apparent viscosity, especially at very low shear rates, the regularization of viscosity in CFD code has been done by defining a threshold shear rate as a 1/1000 value of the critical shear rate, $\dot{\gamma}_y$. Below this value, a linear finite approximation of viscosity was used instead of the H–B model as described in Section 1. INTRODUCTION.

CFD simulations were carried out for the laminar flow of tested CU30 microgels in the steady-state mode. Rotational impeller movement was simulated using a *Multiple Reference Frame* (MRF) method. The boundary conditions for the flow domain were defined in the ANSYS Fluent code as *Wall* for the tank wall and bottom, impeller and shaft, and *Symmetry* for the free surface of the stirred liquid to mimic the zero shear stress there. The set of transport equations was discretized using the finite volume method and solved using the second order upwind scheme. The simulations were considered complete after reaching the convergence represented by a plateau of the numerical sum of residues. The number of iterations needed to achieve the plateau of residuals was dependent on the simulated flow problem and reached a maximum of 13,000. Numerical simulations were carried out using a high-performance computing server. The server consisted of two Intel Xeon Gold 5122 processors (8C/16T, at 3.6 GHz) and 256 GB of quad-channel ECC DDR4 RAM.

3.2. Numerical results

The results of numerical simulations are presented in the same way as the experimental results, in the form of tangential and axial forces (Figs. 7a, 8a) and the related dimensionless criteria, i.e. the power number and the axial thrust number (Figs. 7b, 8b). In order to determine the tangential forces, as in the experiment, the method based on the primary torque exerted by the impeller on the stirred liquid was used. Values of the T_o were read from the modelling results, and then tangential force, mixing power and power number were calculated. In the case of axial forces, it was possible to read their values directly from the results of CFD simulations, therefore it was necessary to calculate only the axial thrust number.

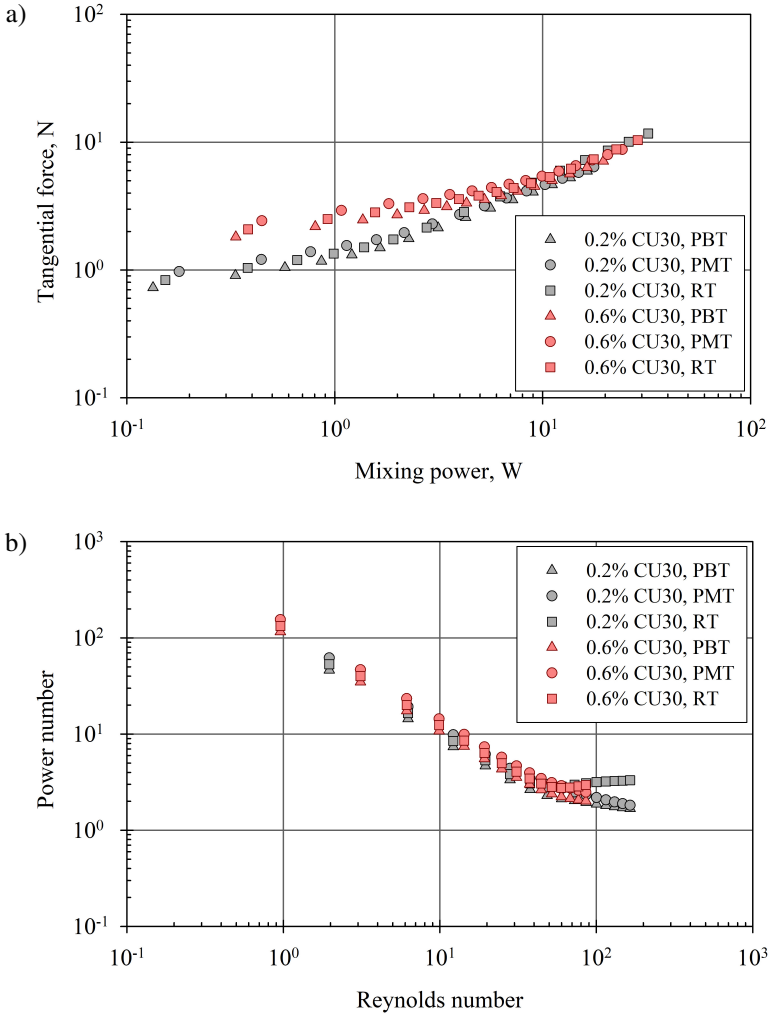

Fig. 7. Tangential forces generated by the impellers (a) and mixing power characteristics (b) of studied systems. CFD numerical data

Analysing results presented in Figures 7 and 8 obtained from the modelling it was found that qualitatively they are very similar to those obtained from the experiments. Values of both tangential and axial forces increased with increasing value of mixing power in the whole range of P. The power number in the laminar flow regime decreased linearly with slope of $a = -0.998$ and was dependent on the impeller type in the transitional flow range, while the axial thrust number first decreased, and then increased from about Re = 115. Moreover, it was found that results obtained from CFD are more regular than these from experiments, which can be found especially by the examination of tangential force charts. Systematic results from CFD may be related to the elimination of deviations occurring during the measurements, resulting, for example, from the random errors of the used measuring devices.

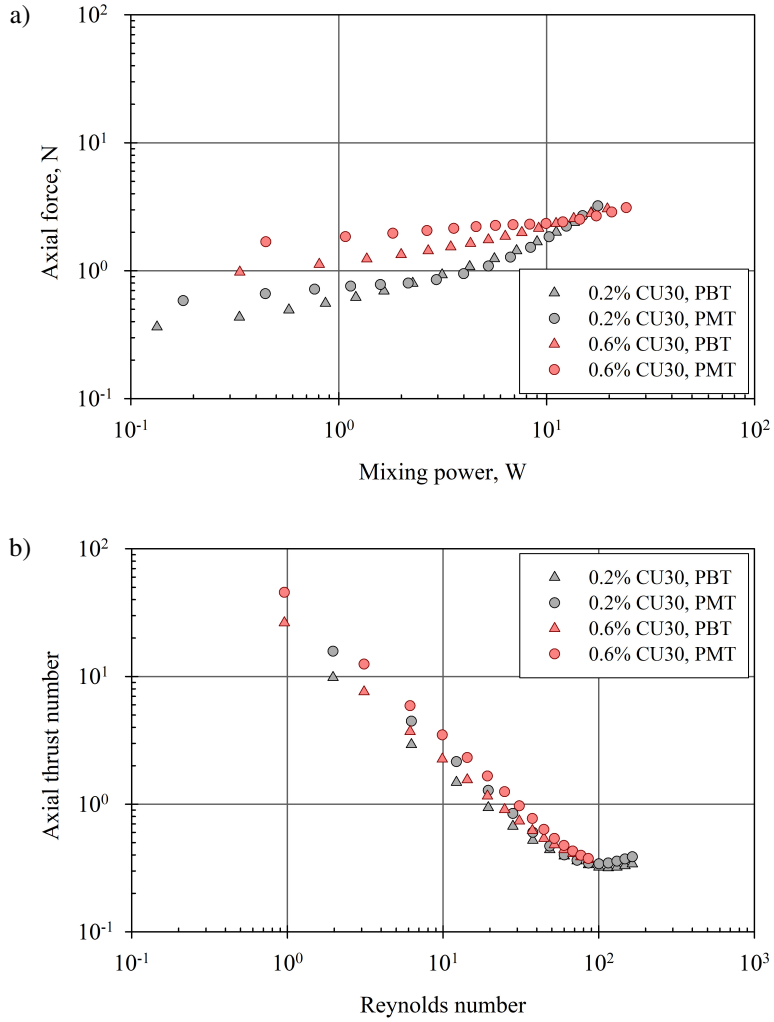

Fig. 8. Axial forces generated by the impellers (a) and dimensionless axial thrust number (b). CFD numerical data

Overall comparison of experimental and numerical results showed that there is a good agreement between them. Qualitative assessment, however, is not sufficient to the unequivocal decision about the correctness of particular modelling. Therefore, in order to quantify the correctness of the adopted method of simulations, the numerical results were validated using the experimental data. The validation results are presented in the next section of this paper.

4. DISCUSSION

4.1. Validation

The results obtained from CFD numerical simulations in the form of tangential and axial forces were compared quantitatively with the analogous results determined in the experimental study. The percentage relative deviation, δ, between the experimental and predicted values of tested parameters was used as a measure of agreement. Values of δ_i were calculated for consecutive impeller speeds, N = 60–900 rpm, from the equation:

$$\delta_i = \frac{X_{\mathrm{exp},i} - X_{\mathrm{CFD},i}}{X_{\mathrm{exp},i}} \cdot 100\% \tag{3}$$

where X denotes one of the analysed parameters: f_φ or f_{ax}. Then, calculated values of δ_i were averaged for successive impeller speeds. Average values of the relative deviation for all mixing tanks and two microgels are collected in Table 3.

Table 3. Percentage relative deviation, δ, between the experimental and predicted data

Impeller type	δ, %			
	0.2% CU30		0.6% CU30	
	f_φ	f_{ax}	f_φ	f_{ax}
PBT	1.2	0.3	–2.1	–2.9
PMT	1.6	3.0	–3.1	–3.7
RT	–2.6	–	–1.5	–

The average relative deviations, collected in Table 3, were both negative and positive. It means that a part of the CFD results was underestimated and a part of them overestimated compared to the experiment. It was found that in the case of 0.2% CU30 microgel the numerical results were moderately overestimated for PBT and PMT impellers, and underestimated for RT, while for 0.6% CU30 all the data from modelling were slightly underestimated.

In the comparison of tangential forces, the smallest value of average relative deviation (1.2%) was obtained for PBT impeller and 0.2% CU30, whereas the highest (-3.1%) for PMT type impeller and 0.6% concentration of the polymer. The same tendency was observed in the case of axial forces – the smallest value of δ (0.3%) was noted for PBT and 0.2% CU30, while the highest (–3.7%) for PMT and 0.6% microgel. Taking into account the overall results, it should be stated that values of average relative deviation ranged from –3.7% to 3.0%. Such values prove a satisfactory agreement between the compared experimental and numerical results. Therefore it can be concluded that the adopted methodology of numerical simulations is correct and valid.

4.2. Resultant force

Values of the resultant force, obtained in this study, were compared with literature data (Story et al., 2018). The experiment described in the literature was performed in a mixing tank with a diameter of $T = 222$ mm, equipped with four flat baffles and a PMT type impeller with a diameter of $D = 0.078$ m. One of the tested fluids was 0.2 wt% Carbopol 940 (C940) with pH ≈ 5.1. Comparing the obtained from H–B model theoretical rheological characteristics of literature liquid and the Carbopol microgels tested in this study (Figure 9), it was found that for a particular value of $\dot{\gamma}$, C940 was characterized by the lowest value of apparent viscosity (except for a very narrow $\dot{\gamma}$ range where μ_{app} for C940 was higher than for 0.2% CU30, due to the higher value of yield point).

Analysis of the resultant forces presented in Figure 10 showed that for low values of mixing power, the differences between values of F obtained for the presented mixing tanks are significant. However, as the value of P increased, the differences gradually decreased. The resultant force for different systems of a tank – impeller – liquid is comparable for $P > 10$ W. Nevertheless, presented data shows that among the two tested impellers, the PMT was the one that produced higher resultant force. On the other hand, comparing results for one type of impeller it was concluded that the resultant force increased with increasing value of apparent viscosity. Except for the literature data for Carbopol 940, Figure 10 shows also the literature exponential model $F = 1.31P^{0.67}$ that describes with a very good agreement resultant forces in the same stirred tank filled with water, 0.2% CMC, glucose syrup solutions with viscosities 0.012 and 0.13 Pa s,

respectively, and 0.2% C940 for $P > 0.6$ W. Comparing these literature data to the results obtained in this study it can be concluded that the slope of a plotted line is in good accordance with experimental data for CU30 for $P > 10$ W. However, points representing the actual experiments are placed visibly below. The exact form of exponential model determined for stirred tanks tested in this study and power draw of $P > 10$ W is $F = 1.03P^{0.68}$. A potential reason for lowering the value of the resultant force for a certain range of mixing power may be the lack of baffles in the tested stirred tanks, compared to the literature vessel.

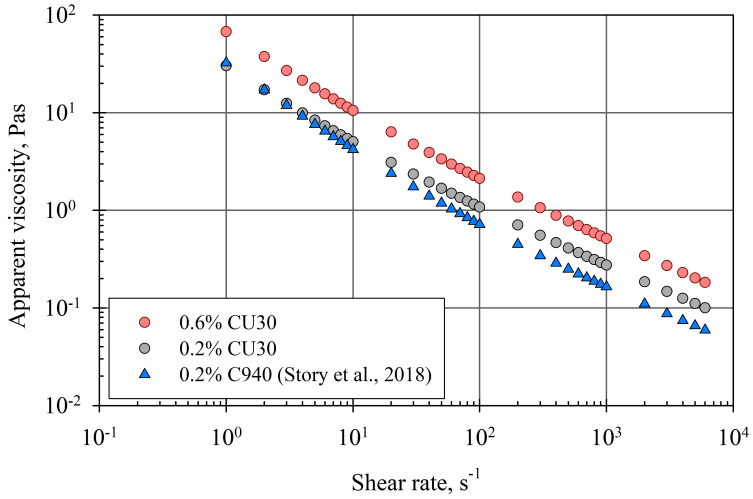

Fig. 9. Apparent viscosity of three Carbopol microgels

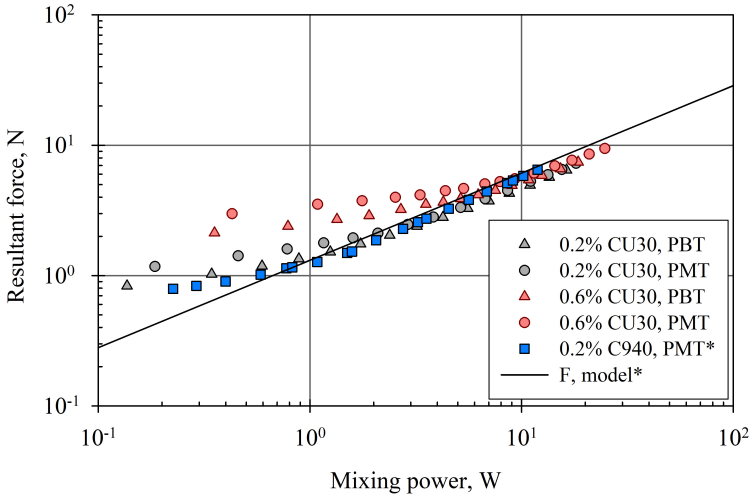

Fig. 10. Resultant force generated in stirred tanks (*data from literature (Story et al., 2018))

5. CONCLUDING REMARKS

Based on the literature review, the tangential and axial forces exerted by the rotating impeller on the stirred material play an important role in creating a proper circulation inside the stirred tank that ensures the required homogeneity of the mixture. It is especially important for yield-stress fluids since high shear forces occurring near the rotating impeller lead to the generation of an intensive mixing zone called a cavern. Outside this well-mixed zone, the fluid is practically stagnant, which prevents it from obtaining its homogeneity.

The presented research on stirring of yield-stress fluids includes broad experimental and numerical investigation of tangential and axial forces created in the mixing tank equipped with the radial (RT) or axial (PMT) or mixed (PBT) type of the impeller.

The tangential force was calculated from measured torque. It was found that both the impeller type and the rheological properties of CU30 microgel have an impact on the tangential forces. The smallest values of f_φ were observed for PBT impeller, while the highest ones were usually for the PMT type impeller. Higher tangential forces were produced for 0.6% CU30 than for 0.2% CU30, but the polymer concentration effect was visible clearly for $P < 10$ W.

The axial force was calculated from measured apparent mass of the stirred tank but only for PBT and PMT impellers since the RT did not exert a measurable axial thrust. Similar to the tangential force, the axial force increased with growing power draw. In general, although higher values of the axial force were observed for the PMT impeller and 0.6% CU30, the differences between axial forces for tested impellers faded with increasing power draw.

Determination of the tangential and axial forces led to calculation of the resultant tangential-axial force. It was found that although the axial force was smaller than the tangential force, both components had a considerable impact on the resultant force, and therefore also on the circulation of the material in the stirred tank. The PMT type impeller produced a higher resultant force than PBT. Also, the resultant force increased with increasing value of apparent viscosity. Comparison of the estimated resultant force to the literature data revealed a satisfying agreement for power draw $P > 10$ W. Slight differences between the authors' own and literature data can result from different geometries of the tank, i.e. the lack of baffles.

An important part of undertaken research was connected with determination of tangential and axial forces from CFD numerical simulations. The tangential force, similar to the experimental one, was calculated from the predicted value of torque, while the axial force was read directly from CFD results. Generally, numerical results were positively validated using the experimental data. The maximum absolute value of percentage relative deviation between the experimental and predicted values of f_φ and f_{ax} did not exceed 3.7%. Thus, it can be concluded that simulations were performed correctly. Therefore, the adopted methodology of numerical simulations can be recommended in further analysis of yield-stress fluid flow in stirred tanks.

SYMBOLS

a	exponent
$A,\ B$	constants in Eq. (2)
c_{CU30}	percent weight concentration, wt%
D	impeller diameter, m
d	shaft diameter, m
F	total force, N
f_{ax}	axial force, N
f_φ	tangential force, N
H	level of liquid in the tank, m
k	consistency coefficient, Pa·s^n
N	impeller speed, s^{-1}
n	flow index
P	mixing power, W
Po	power number

R	impeller radius, m
Re	generalized Reynolds number
T	tank diameter, m
T_o	primary torque, N·m
t	temperature, °C
Th	thrust number
z	distance from the tank bottom to the impeller centre, m

Greek symbols

$\dot{\gamma}$	shear rate, s^{-1}
δ	mean square deviation, ‰
μ	dynamic viscosity, Pa·s
τ	shear stress, Pa
τ_y	yield stress, Pa

Subscripts

app	apparent value
exp	value from experiment
CFD	value from numerical simulation
t	threshold value

ACKNOWLEDGMENTS

The study was carried out within the research project No.2017/25/B/ST8/01693 funded by the National Science Centre Poland.

REFERENCES

Adams L. W., Barigou M., 2007. CFD analysis of caverns and pseudo-caverns developed during mixing of non-Newtonian fluids. *Chem. Eng. Res. Des.*, 85, 598–604. DOI: 10.1205/cherd06170.

Amanullah A., Hjorth S.A., Nienow A.W., 1997. Cavern sizes generated in highly shear thinning viscous fluids by SCABA 3SHP1 impellers. *Food Bioprod. Process.*, 75, 232–238. DOI: 10.1205/096030897531630.

Amanullah A., Hjorth S.A., Nienow A.W., 1998. A new mathematical model to predict cavern diameters in highly shear thinning, power law liquids using axial flow impellers. *Chem. Eng. Sci.*, 53, 455–469. DOI: 10.1016/S0009-2509(97)00200-5.

Ameur H., 2016. Agitation of yield stress fluids in different vessel shapes. *Eng. Sci. Technol.*, 19, 189–196. DOI: 10.1016/j.jestch.2015.06.007.

Ameur H., 2017. Mixing of a viscoplastic fluid in cylindrical vessels equipped with paddle impellers. *Chemistry Select*, 2, 11492–11496. DOI: 10.1002/slct.201702459.

Ameur H., 2019. Some modifications in the Scaba 6SRGT impeller to enhance the mixing characteristics of Hershel-Bulkley fluids. *Food Bioprod. Process.*, 117, 302–309. DOI: 10.1016/j.fbp.2019.08.007.

Ameur H., Bouzit M., Helmaoui M., 2011. Numerical study of fluid flow and power consumption in a stirred vessel with a Scaba 6SRGT impeller. *Chem. Process Eng.*, 32, 351–366. DOI: 10.2478/v10176-011-0028-0.

Arratia P.E., Kukura J., Lacombe J., Muzzio F.J., 2006. Mixing of shear-thinning fluids with yield stress in stirred tanks. *AIChE J.*, 52, 2310–2322. DOI: 10.1002/aic.10847.

Bakker C.W., Meyer C.J., Deglon D.A., 2009. Numerical modelling of non-Newtonian slurry in a mechanical flotation cell. *Miner. Eng.*, 22, 944–950. DOI: 10.1016/j.mineng.2009.03.016.

Bakker C.W., Meyer C.J., Deglon D.A., 2010. The development of a cavern model for mechanical flotation cells. *Miner. Eng.*, 23, 968–972. DOI: 10.1016/j.mineng.2010.03.016.

Bhole M.R., Bennington C.P.J., 2010. Performance of four axial flow impellers for agitation of pulp suspensions in a laboratory-scale cylindrical stock chest. *Ind. Eng. Chem. Res.*, 49, 4444-4451. DOI: 10.1021/ie901854d.

Bhole M.R., Hui L.K., Gomez C., Bennington C.P.J., Dumont G.A., 2011. The effect of off-wall clearance of a side-entering impeller on the mixing of pulp suspensions in a cylindrical stock chest. *Can. J. Chem. Eng.*, 89, 985–995. DOI: 10.1002/cjce.20503.

Bonn D., Denn M.M., Berthier L., Divoux T., Manneville S., 2017. Yield stress materials in soft condensed matter. *Rev. Mod. Phys.*, 89, 035005, 1–40. DOI: 10.1103/RevModPhys.89.035005.

del Pozo D.F., Line A., Van Geem K.M., Le Men C., Nopens I., 2020. Hydrodynamic analysis of an axial impeller in a non-Newtonian fluid through particle image velocimetry. *AIChE J.*, 66, e16939, 1–16. DOI: 10.1002/aic.16939.

Dylak A., Jaworski Z., 2015. A CFD study of formation of the intensive mixing zone in a highly non-Newtonian fluid. *AIP Conference Proceedings*, 1648, 030013. DOI: 10.1063/1.4912330.

Ford C., Ein-Mozaffari F., Bennington C.P.J., Taghipour F., 2006. Simulation of mixing dynamics in agitated pulp stock chests using CFD. *AIChE J.*, 52, 3562–3569. DOI: 10.1002/aic.10958.

Fořt I., Seichter P., Pešl L., 2013. Axial thrust of axial flow impellers. *Chem. Eng. Res. Des.*, 91, 789–794. DOI: 10.1016/j.cherd.2012.10.001.

Frigaard I. A., Nouar C., 2005. On the usage of viscosity regularisation methods for visco-plastic fluid flow computation. *J. Non-Newtonian Fluid Mech.*, 127, 1-26. DOI: 10.1016/j.jnnfm.2005.01.003.

Galindo E., Arguello M., Velasco D.A., Albiter V., Martinez A., 1996. A comparison of cavern development in mixing a yield stress fluid by Rushton and intermig impellers. *Chem. Eng. Technol.*, 19, 315–323. DOI: 10.1002/ceat.270190405.

Galindo E., Nienow A.W., 1992. Mixing of highly viscous simulated Xanthan fermentation broths with the Lightinin A-315-impeller. *Biotechnol. Prog.*, 8, 233–239. DOI: 10.1021/bp00015a009.

Herschel W. H., Bulkley R., 1926. Consistency measurements of rubber-benzol solutions. *Kolloid-Zeitschrift*, 39, 291–300. DOI: 10.1007/BF01432034.

Hui L.K., Bennington C.P.J., Dumont G.A., 2009. Cavern formation in pulp suspensions using side-entering axial-flow impellers. *Chem. Eng. Sci.*, 64, 509–519. DOI: 10.1016/j.ces.2008.09.021.

Jaworski Z., Nienow A.W., 1994. LDA measurements of flow fields with hydrofoil impellers in fluids with different rheological properties. *Eighth European Conference on Mixing*, *IChemE Symp. Series*, 136, 105–112.

Jaworski Z., Spychaj T., Story A., Story G., 2021. Carbomer microgels as model yield-stress fluids. *Rev. Chem. Eng.*, 000010151520200016. DOI: 10.1515/revce-2020-0016.

Kelly W., Gigas B., 2003. Using CFD to predict the behavior of power law fluids near axial-flow impellers operating in the transitional flow regime. *Chem. Eng. Sci.*, 58, 2141–2152. DOI: 10.1016/S0009-2509(03)00060-5.

Nienow A.W., Elson T.P., 1988. Aspects of mixing in rheologically complex fluids. *Chem. Eng. Res. Des.*, 66, 5–15.

Rodriguez B.E., Wolfe M.S., Fryd M., 1994. Nonuniform swelling of alkali swellable microgels. *Macromolecules*, 27, 6642–6647. DOI: 10.1021/ma00100a058.

Russell A.W., Kahouadji L., Mirpuri K., Quarmby A., Piccione P.M., Matar O.K., Luckham P.F., Markides C.N., 2019. Mixing viscoplastic fluids in stirred vessels over multiple scales: A combined experimental and CFD approach. *Chem. Eng. Sci.*, 208, 115129. DOI: 10.1016/j.ces.2019.07.047.

Savreux F., Jay P., Magnin A., 2007. Viscoplastic fluid mixing in a rotating tank. *Chem. Eng. Sci.*, 62, 2290–2301. DOI: 10.1016/j.ces.2007.01.020.

Simmons M.J.H., Edwards I., Hall J.F., Fan X., Parker D.J., Stitt E.H., 2009. Techniques for visualization of cavern boundaries in opaque industrial mixing systems. *AIChE J.*, 55, 2765–2772. DOI: 10.1002/aic.11889.

Sossa-Echeverria J., Taghipour F., 2014. Effect of mixer geometry and operating conditions on flow mixing of shear thinning fluids with yield stress. *AIChE J.*, 60, 1156–1167. DOI: 10.1002/aic.14309.

Sossa-Echeverria J., Taghipour F., 2015. Computational simulation of mixing flow of shear thinning non-Newtonian fluids with various impellers in a stirred tank. *Chem. Eng. Process.*, 93, 66–78. DOI: 10.1016/j.cep.2015.04.009.

Story A., Jaworski Z., 2017. A new model of cavern diameter based on a validated CFD study on stirring of a highly shear-thinning fluid. *Chem. Pap.*, 71, 1255–1269. DOI: 10.1007/s11696-016-0119-y.

Story A., Jaworski Z., Major-Godlewska M., Story G., 2018. Influence of rheological properties of stirred liquids on the axial and tangential forces in a vessel with a PMT impeller. *Chem. Eng. Res. Des.*, 138, 398–404. DOI: 10.1016/j.cherd.2018.09.006.

Story A., Story G., Jaworski Z., 2020. Effect of carbomer microgel pH and concentration on the Herschel–Bulkley parameters. *Chem. Process Eng.*, 41, 173–182. DOI: 10.24425/cpe.2020.132540.

Stręk F., 1981. Mieszanie i mieszalniki. Wydawnictwa Naukowo-Techniczne, Warszawa.

Wichterle K., Wein O., 1975. Agitation of concentrated suspensions. CHISA ’75, Paper B.4.6. Prague, Czechoslovakia.

Wu J., Pullum L., 2000. Performance analysis of axial-flow mixing impellers. *AIChE J.*, 46, 489–498. DOI: 10.1002/aic.690460307.

Xiao Q., Yang N., Zhu J. H., Guo L.J., 2014. Modeling of cavern formation in yield stress fluids in stirred tanks. *AIChE J.*, 60, 3057–3070. DOI: 10.1002/aic.14470.

Received 27 May 2021
Received in revised form 16 July 2021
Accepted 19 July 2021